An analytical model to predict stress fields around broken fibres and their effect on the longitudinal failure of hybrid composites

Jose M. Guerrero[a,*], Rodrigo P. Tavares[a,b,c], Fermin Otero[c,d], Joan A. Mayugo[a], Josep Costa[a], Albert Turon[a], Pedro P. Camanho[b,c]

[a]*AMADE, Polytechnic School, Universitat de Girona, Campus Montilivi s/n, E-17003 Girona, Spain*
[b]*DEMec Faculdade de Engenharia, Universidade do Porto, Rua Dr. Roberto Frias, 4200-465 Porto, Portugal*
[c]*INEGI, Rua Dr. Roberto Frias, 400, 4200-465 Porto, Portugal*
[d]*Centre Internacional de Mètodes Numèrics a l'Enginyeria (CIMNE), Edifici C1, Campus Nord UPC C/ Gran Capità S/N, 08034 Barcelona, Spain*

Abstract

This paper presents an analytical model to predict the stress redistribution around broken fibres in hybrid polymer composites. The model is used under the framework of a progressive failure approach to study the load redistribution around breaks in hybrid composites. The outcomes of the model are validated by comparing it with a spring element model. Moreover, the approach is further used to study the tensile behaviour of different hybrid composites. The results obtained show that the load redistribution around breaks depends on the stiffness ratio between both fibres as well as the matrix behaviour considered and the hybrid volume fraction. Furthermore, the different material parameters have a large effect on the tensile behaviour, with an increase of ductility achieved if the failure process of the two fibres is gradual.

Keywords: Stress concentration, Hybrid composites, Modelling, Micro-mechanics

1. Introduction

Fibre hybridization is a potential solution to the quasi-brittle behaviour of fibre reinforced polymers (FRP), resulting in fibre tensile failure with hardly any previous damage symptoms [1–5]. In a hybrid composite, a Low Elongation (LE) fibre is combined with a High Elongation (HE) fibre. This combination may lead to a larger failure strain of

*Corresponding author. Tel.: +34 972 41 88 17.
Email address: `josemanuel.guerrero@udg.edu` (Jose M. Guerrero)

baseline composites based on LE fibres, resulting in a hybrid effect. Moreover, the failure process of the material can become gradual leading to an increase of ductility [6, 7]. It is currently accepted that progressive failure, dynamic effects, and thermal residual stresses are the main reasons to explain the hybrid effect [4, 8, 9].

The strength of the fibres is not deterministic and follows a statistical distribution. When a fibre fails, the fibre locally loses its loading capability, which is recovered by shear transfer in the matrix over a distance called ineffective length. In this region the neighbour intact fibres are subjected to stress concentrations. As the load is incremented, clusters of broken fibres are created increasing the stress concentration in intact fibres even further. In a non-hybrid composite this process quickly leads to final failure, whilst in a hybrid composite the stress redistribution around broken fibres is altered due to the presence of fibres with different mechanical and geometrical properties [10]. These differences may alter and delay the formation of clusters leading to hybrid effects [11–13]. However, it remains to be understood if final failure happens either by the accumulation of damage and clusters or by the unstable propagation of a large critical cluster [4].

Different models that attempt to represent the failure process of composite materials and the stress redistribution around breaks are available in the literature. These models can be classified as Global Load Sharing (GLS) and Local Load Sharing (LLS). In GLS models, the stress loss by a broken fibre is redistributed equally among all intact fibres [1, 14–17]. As a consequence, such models cannot predict the formation of clusters, which in general leads to a large overprediction of the failure strength. Nonetheless, GLS models can capture some trends affecting the failure process such as fibre fragmentation or the effect of the fibre strength variation [18, 19].

In the LLS models, the load of broken fibres is redistributed into the closest intact fibres allowing to capture the formation of clusters. In these models, different modelling approaches exist [20]: analytical models [21–23], spring element models [24–26], fibre bundle models [2, 11] and micromechanical finite element models [18, 27, 28]. Though all methods, in general, predict the failure strength accurately, all predict different cluster formation and evolution due to the different modelling strategies. Moreover, all models omit the dynamic effects and overpredict the fibre break density compared with experiments [3, 4].

Currently there is not any analytical model that can predict accurately the Stress Concentration Factor (*SCF*) around clusters of broken fibres in hybrid composites taking into account the differences in elastic and geometrical properties of the two fibres in the hybrid [10]. Moreover, in depth parametric analysis of the load redistribution around breaks in hybrid composites, and their effect on the tensile response still remain scarce [2, 11, 12, 18, 24]. Furthermore, recent simulations showed that the load redistribution around breaks in non-hybrid composites is heavily influenced by the matrix behaviour [20]. However, such effects have not been studied with hybrid composites. It is, therefore, vital to further understand the load redistribution and to improve the available tools to predict this load redistribution as this is believed to be the main mechanism that triggers final failure of composites.

In this work, a new analytical model to compute the load redistribution around a cluster of broken fibres in a hybrid composite is presented. The model is an extension of the non-hybrid model presented in St-Pierre *et al.* [22]. The analytical model is used within the framework of a progressive failure model approach [2] to study the load redistribution around broken fibres in different hybrid composites using both a plastic and an elastic matrix. The model is validated by comparing with the extension of the Spring Element Model (SEM) to hybrid composites proposed by Tavares *et al.* [24]. Furthermore, the tensile failure of different hybrid composites is simulated using the same approach with the objective of understanding the influence of the modelling parameters on the macroscopic response. These simulations are also validated and compared with the SEM.

2. Modelling strategy

In this work, a new analytical model to predict the *SCF* around broken fibres in hybrid composites is presented. The analytical model is used within the framework of a Progressive Failure Model (PFM) [2]. In the PFM, a three dimensional Representative Volume Element (RVE) containing a random distribution of fibres is used. By applying known functions to predict the load redistribution around broken fibres, the PFM can simulate the tensile failure process of composite materials, capturing fibre clustering, fibre fragmentation and stiffness loss. This model is reviewed in the next sections where also the new analytical model to predict the *SCF* around breaks is presented.

To validate the new proposed model used in PFM, the obtained results are compared with the SEM. The SEM was firstly developed by Okabe *et al.* [25, 26, 29] and was recently extended to hybrid composites, damageable interfaces, and random fibre microstructures by Tavares *et al.* [24]. The SEM consists of a more complex three dimensional RVE where the fibres are longitudinal tensile springs connected by transverse springs representing the matrix. Unlike the PFM, the SEM can predict the load redistribution around breaks inherently from the equilibrium equations, being a finite element model. However, SEM is computationally more expensive than PFM. Further details of the SEM can be seen in Tavares *et al.* [24].

2.1. Progressive Failure Model

The PFM consists of a RVE of width a, height b and length L containing a random distribution of fibres of a given radius. The fibres are divided into elements of length l along their longitudinal direction, leading to a succession of planes. Each fibre is denoted with the sub-index $q \in \left[1, ..., N_q\right]$, while each plane is denoted with the sub-index $p \in \left[1, ..., N_p\right]$, where N_q and N_p are the number of fibres and planes respectively, see Figure 1. Each element has a different strength according to a statistical distribution. Once an element fails, a damage distribution is applied over the ineffective length of the broken fibre, whereas stress concentration is applied into the neighbouring intact fibre elements.

2.1.1. Constitutive equation

The constitutive equation relating the stress of each element, $\sigma_{p,q}$, and the strain ε_p is

$$\sigma_{p,q} = \frac{SCF_{p,q}}{\Omega_p} E_q \left(1 - D_{p,q}\right) \varepsilon_p \tag{1}$$

where $SCF_{p,q}$ is the stress concentration factor of element p, q, E_q is the Young's modulus of fibre q, $D_{p,q}$ is the state damage variable, which is equal to 1 for broken elements, equal to 0 for intact elements and in between for elements in any stress recovery, ε_p is the strain of the plane (which is considered to be the same for all elements of plane p) and Ω_p is a stress ratio which enforces load equilibrium by modifying the stress concentration according to the strain level. Readers are referred to Guerrero *et al.* [2] for an in-depth description of the model.

The evolution of $D_{p,q}$ and $SCF_{p,q}$, depends on the model used to predict the ineffective length and the *SCF* around breaks, respectively. Even though any model may be applied to predict both, it is important to use models that are consistent for both parameters. In the following section, the model to predict damage is explained, whereas the new model for predicting the *SCF* is explained in Section 2.1.3.

2.1.2. Functions for ineffective length

In this work two different behaviours to simulate damage are considered, i.e. the matrix is plastic or the matrix is elastic.

When the matrix is plastic, a modified version of Kelly-Tyson shear-lag model [30] is adapted as given in St-Pierre *et al.* [22]. This approach adds a factor, H, which scales the ineffective length with cluster size. Here, two broken fibre elements belong to the same cluster (c), if the distance between the centres of both fibres is below four times the fibre radius and both elements are in the same plane p. Each cluster is represented with the sub-index p, c, with $c \in \left[1, ..., N_p^{\mathrm{c}}\right]$ where N_p^{c} is the number of clusters at plane p. This means that the scaling effects depend on the element length, l. Nonetheless, it was verified that varying the element length does not significantly change neither the macroscopic response of the composite nor the damage development. The ineffective length of a broken fibre in cluster p, c is then

$$L_{p,q}^{\mathrm{in}} = \frac{R_q E_q}{2\tau_q} H_{p,c} \varepsilon_p = \frac{n_{p,c} \pi R_q^2 E_q}{C_{p,c} \tau_q} \varepsilon_p \tag{2}$$

where τ_q is the matrix shear yield stress, R_q is the fibre radius, $C_{p,c} = 4s\sqrt{n_{p,c}}$, where $n_{p,c}$ is the number of broken fibres on cluster p, c and s is the mean centre-to-centre distance between each fibre and its closest neighbour. Here, it is estimated with $s = \left(\left(R_{\mathrm{f1}} V_{\mathrm{f1}} + R_{\mathrm{f2}} V_{\mathrm{f2}}\right) / V_{\mathrm{f}}\right) \sqrt{\pi / V_{\mathrm{f}}}$, where R_{f1} and R_{f2} are the fibre radius of fibre populations 1 and 2 respectively, V_{f} is the overall fibre volume fraction and V_{f1} and V_{f2} are the fibre volume fraction of each population respectively ($V_{\mathrm{f}} = V_{\mathrm{f1}} + V_{\mathrm{f2}}$). It is worth mentioning that here, s, is not the average inter-fibre spacing of the cluster, but the average inter-fibre spacing of the overall RVE. That is, because the ineffective length should depend not only on the fibres in the broken cluster but also on the fibres that surround it.

The damage of element p, q according to each break in the fibre q at each plane i

follows a linear recovery with

$$D_{p,q} = \begin{cases} \max\left(\dfrac{L^{\text{in}}_{i,q} - |i-p|\, l}{L^{\text{in}}_{i,q}}\right) & \forall i : \left(D_{i,q} = 1\right) \cup \left(|i-p|\, l < L^{\text{in}}_{i,q}\right) \\ 0 & \text{otherwise.} \end{cases} \tag{3}$$

If the matrix behaves elastically, the Cox's shear-lag model [31, 32] is adapted as in [20]. Then the ineffective length is

$$L^{\text{in}}_{p,q} = \frac{H_{p,c} E_q}{2G_{\text{m}}}\left(s - 2\frac{R_{\text{f1}} V_{\text{f1}} + R_{\text{f2}} V_{\text{f2}}}{V_{\text{f}}}\right)(-\ln 0.001)\,\sqrt{\frac{2G_{\text{m}} R_q}{E_q\left(s - 2\dfrac{R_{\text{f1}} V_{\text{f1}} + R_{\text{f2}} V_{\text{f2}}}{V_{\text{f}}}\right)}} \tag{4}$$

where G_{m} is the matrix shear modulus. It should be noted that this length corresponds to a recovery of 99.9% of the fibre stress [20]. The damage is then computed with

$$D_{p,q} = \begin{cases} \max\left(\exp\left(-\dfrac{|i-p|\, l}{H_{p,c} R_q}\sqrt{\dfrac{2G_{\text{m}} R_q}{E_q\left(s - 2\dfrac{R_{\text{f1}} V_{\text{f1}} + R_{\text{f2}} V_{\text{f2}}}{V_{\text{f}}}\right)}}\right)\right) & \forall i : \left(D_{i,q} = 1\right) \cup \left(|i-p|\, l < L^{\text{in}}_{i,q}\right) \\ 0 & \text{otherwise.} \end{cases} \tag{5}$$

2.1.3. Stress concentration factor model

Different approaches have been used to predict the *SCF* around breaks [3, 22, 33, 34]. Recently, St-Pierre *et al.* [22] presented a model capable of predicting the *SCF* around coplanar clusters of broken fibres in non-hybrid composites. St-Pierre's *et al.* [22] approach is adapted and extended here to work with hybrid composite materials. The reason why this model was chosen over others is related to the fact that the model predicts the *SCF* around clusters instead of isolated fibre breaks, and it is built on a simple but solid physical background. The model assumes that the *SCF* around a cluster of broken fibres takes a power-law shape.

In this work, the increment of *SCF* for an intact element p, q due to cluster i, c is represented with two functions, δ and λ, so that $\Delta SCF = \delta \cdot \lambda$. The function δ depends on the in-plane distance $\left(r_{q-c}\right)$ between the geometrical centre of coordinates of cluster i, c and intact element p, q, while λ depends on the plane position along the ineffective length. As each cluster may contain broken fibres of each type, an intact element may receive *SCF* from broken fibres of the same population or the other, leading to four combinations of δ

$$\begin{aligned} \delta_{11_{(q-c)}} &= I_{11_{i,c}}\left(\frac{R_{i,c}}{r_{q-c}}\right)^{\alpha} & \qquad \delta_{22_{(q-c)}} &= I_{22_{i,c}}\left(\frac{R_{i,c}}{r_{q-c}}\right)^{\alpha} \\ \delta_{12_{(q-c)}} &= I_{12_{i,c}}\left(\frac{R_{i,c}}{r_{q-c}}\right)^{\alpha} & \qquad \delta_{21_{(q-c)}} &= I_{21_{i,c}}\left(\frac{R_{i,c}}{r_{q-c}}\right)^{\alpha} \end{aligned} \tag{6}$$

where $\delta_{11_{(q-c)}}$ and $\delta_{22_{(q-c)}}$ represent the increment of SCF that an intact element of fibre population 1 and 2 respectively receives due to broken fibres of its own type in cluster i, c, while $\delta_{12_{(q-c)}}$ and $\delta_{21_{(q-c)}}$ are the increment of SCF that an element of fibre population 1 and 2 respectively receives due to broken fibres of different type in cluster i, c. $R_{i,c}$ is the equivalent radius of the cluster, estimated with $\pi R_{i,c}^2 = n_{i,c} S_{i,c}^2$, where $S_{i,c}$ is the average fibre spacing of the cluster, $S_{i,c} = \left(\left(n_{1_{i,c}} R_{\mathrm{f}1} + n_{2_{i,c}} R_{\mathrm{f}2}\right) / n_{i,c}\right) \sqrt{\pi / V_{\mathrm{f}}}$, where $n_{1_{i,c}}$ and $n_{2_{i,c}}$ are the number of broken fibres of population 1 and 2 respectively in cluster i, c and $n_{i,c} = n_{1_{i,c}} + n_{2_{i,c}}$. The exponent α is an input parameter which controls the maximum value of SCF and the shape of the curve. According to the literature, this value can be adopted as $\alpha = 2$ for a plastic matrix and $\alpha = 3.8$ for elastic matrix [20, 22]. The terms I are constants, which are determined later in this section, see Eq. (10).

Similarly, as there are two fibre populations, each cluster i, c has two ineffective lengths, the ineffective length of broken elements of type 1, $L_{1_{i,c}}^{\mathrm{in}}$, and that of broken elements of type 2, $L_{2_{i,c}}^{\mathrm{in}}$. Therefore, two functions appear for λ as

$$
\begin{aligned}
\lambda_{1_{(p-i)}} &= \begin{cases} \dfrac{L_{1_{i,c}}^{\mathrm{in}} - l\,|i-p|}{L_{1_{i,c}}^{\mathrm{in}}} & \forall (i,c):\ l\,|i-p| < L_{1_{i,c}}^{\mathrm{in}} \qquad \text{Plastic matrix} \\ \exp\left(-\dfrac{|i-p|\, l C_{i,c}}{2\pi n_{i,c} R_{\mathrm{f}1}^2} \sqrt{\dfrac{2 G_{\mathrm{m}} R_{\mathrm{f}1}}{E_{\mathrm{f}1}\left(s - 2\dfrac{R_{\mathrm{f}1} V_{\mathrm{f}1} + R_{\mathrm{f}2} V_{\mathrm{f}2}}{V_{\mathrm{f}}}\right)}} \right) & \forall (i,c):\ l\,|i-p| < L_{1_{i,c}}^{\mathrm{in}} \qquad \text{Elastic matrix} \end{cases} \\
\lambda_{2_{(p-i)}} &= \begin{cases} \dfrac{L_{2_{i,c}}^{\mathrm{in}} - l\,|i-p|}{L_{2_{i,c}}^{\mathrm{in}}} & \forall (i,c):\ l\,|i-p| < L_{2_{i,c}}^{\mathrm{in}} \qquad \text{Plastic matrix} \\ \exp\left(-\dfrac{|i-p|\, l C_{i,c}}{2\pi n_{i,c} R_{\mathrm{f}2}^2} \sqrt{\dfrac{2 G_{\mathrm{m}} R_{\mathrm{f}2}}{E_{\mathrm{f}2}\left(s - 2\dfrac{R_{\mathrm{f}1} V_{\mathrm{f}1} + R_{\mathrm{f}2} V_{\mathrm{f}2}}{V_{\mathrm{f}}}\right)}} \right) & \forall (i,c):\ l\,|i-p| < L_{2_{i,c}}^{\mathrm{in}} \qquad \text{Elastic matrix} \end{cases}
\end{aligned}
\tag{7}
$$

where $\lambda_{1_{(p-i)}}$ represents the evolution of $\delta_{11_{(q-c)}}$ and $\delta_{21_{(q-c)}}$ along $L_{1_{i,c}}^{\mathrm{in}}$, while $\lambda_{2_{(p-i)}}$ represents the evolution of $\delta_{22_{(q-c)}}$ and $\delta_{12_{(q-c)}}$ along $L_{2_{i,c}}^{\mathrm{in}}$. $E_{\mathrm{f}1}$ and $E_{\mathrm{f}2}$ are the Young's modulus of fibre type 1 and 2 respectively.

Because of load equilibrium, the load loss of each fibre population in the cluster, must be redistributed into the remaining intact fibres at same plane. Thus, the following equilibrium equations arise

$$
\begin{aligned}
\pi R_{\mathrm{f}1}^2 n_{1_{i,c}} \sigma_1^{\infty} &= \int_{R_{i,c}}^{R_{\mathrm{t}}} I_{11_{i,c}} \left(\frac{R_{i,c}}{r_{q-c}}\right)^{\alpha} \sigma_1^{\infty} V_{\mathrm{f}1} 2\pi r_{q-c}\, \mathrm{d}r_{q-c} + \int_{R_{i,c}}^{R_{\mathrm{t}}} I_{21_{i,c}} \left(\frac{R_{i,c}}{r_{q-c}}\right)^{\alpha} \sigma_2^{\infty} V_{\mathrm{f}2} 2\pi r_{q-c}\, \mathrm{d}r_{q-c} \\
\pi R_{\mathrm{f}2}^2 n_{2_{i,c}} \sigma_2^{\infty} &= \int_{R_{i,c}}^{R_{\mathrm{t}}} I_{22_{i,c}} \left(\frac{R_{i,c}}{r_{q-c}}\right)^{\alpha} \sigma_2^{\infty} V_{\mathrm{f}2} 2\pi r_{q-c}\, \mathrm{d}r_{q-c} + \int_{R_{i,c}}^{R_{\mathrm{t}}} I_{12_{i,c}} \left(\frac{R_{i,c}}{r_{q-c}}\right)^{\alpha} \sigma_1^{\infty} V_{\mathrm{f}1} 2\pi r_{q-c}\, \mathrm{d}r_{q-c}
\end{aligned}
\tag{8}
$$

where R_t is the RVE equivalent radius, $R_t = \sqrt{(a \cdot b)/\pi}$, while σ_1^∞ and σ_2^∞ are the stress at infinite for each fibre population respectively. Assuming that the strain is the same for both fibre populations, $\sigma_1^\infty / E_{f1} = \sigma_2^\infty / E_{f2}$. In addition, it is assumed that two intact fibre elements of different type located at the exact same distance to the same break, receive the same increment of force due to the break. This assumption means that the overload transferred from a break to an intact fibre is independent of both the Young's modulus and the fibre radius of the intact fibre. This fact is supported by the results presented in Swolfs *et al.* [10]. As isostrain conditions are considered, force equality implies that the increment of stress concentration solely depends on the stiffness and cross-sectional area of both fibres leading to

$$I_{21_{i,c}} = \frac{E_{f1} R_{f1}^2}{E_{f2} R_{f2}^2} I_{11_{i,c}} \qquad I_{12_{i,c}} = \frac{E_{f2} R_{f2}^2}{E_{f1} R_{f1}^2} I_{22_{i,c}} \tag{9}$$

These conditions imply that a fibre with lower stiffness located at the same distance to the break is subjected to a higher *SCF* than a fibre with a higher stiffness, which is consistent to the general observations seen in the literature [10, 12]. By substituting the relation between σ_1^∞ and σ_2^∞ and Eq. (9) into Eq. (8), the constants $I_{11_{i,c}}, I_{22_{i,c}}, I_{12_{i,c}}$ and $I_{21_{i,c}}$ are obtained as functions of α:

$$\begin{aligned}
I_{11_{i,c}} &= \begin{cases} \dfrac{n_{1_{i,c}} R_{f1}^2 R_{f2}^2}{2 R_{i,c}^2 \ln\left(R_t / R_{i,c}\right) \left(R_{f1}^2 V_{f2} + R_{f2}^2 V_{f1}\right)} & \text{for } \alpha = 2 \\[2ex] \dfrac{n_{1_{i,c}} R_{f1}^2 R_{f2}^2 R_{i,c}^{-\alpha} (\alpha - 2)}{2 \left(R_{f1}^2 V_{f2} + R_{f2}^2 V_{f1}\right) \left(R_{i,c}^2 \left(1/R_{i,c}\right)^\alpha - R_t^2 \left(1/R_t\right)^\alpha\right)} & \text{otherwise.} \end{cases} \\
I_{21_{i,c}} &= \begin{cases} \dfrac{E_{f1} n_{1_{i,c}} R_{f1}^4}{2 E_{f2} R_{i,c}^2 \ln\left(R_t / R_{i,c}\right) \left(R_{f1}^2 V_{f2} + R_{f2}^2 V_{f1}\right)} & \text{for } \alpha = 2 \\[2ex] \dfrac{E_{f1} n_{1_{i,c}} R_{f1}^4 R_{i,c}^{-\alpha} (\alpha - 2)}{2 E_{f2} \left(\left(R_{f1}^2 V_{f2} + R_{f2}^2 V_{f1}\right) \left(R_{i,c}^2 \left(1/R_{i,c}\right)^\alpha - R_t^2 \left(1/R_t\right)^\alpha\right)\right)} & \text{otherwise.} \end{cases} \\
I_{22_{i,c}} &= \begin{cases} \dfrac{n_{2_{i,c}} R_{f1}^2 R_{f2}^2}{2 R_{i,c}^2 \ln\left(R_t / R_{i,c}\right) \left(R_{f1}^2 V_{f2} + R_{f2}^2 V_{f1}\right)} & \text{for } \alpha = 2 \\[2ex] \dfrac{n_{2_{i,c}} R_{f1}^2 R_{f2}^2 R_{i,c}^{-\alpha} (\alpha - 2)}{2 \left(R_{f1}^2 V_{f2} + R_{f2}^2 V_{f1}\right) \left(R_{i,c}^2 \left(1/R_{i,c}\right)^\alpha - R_t^2 \left(1/R_t\right)^\alpha\right)} & \text{otherwise.} \end{cases} \\
I_{12_{i,c}} &= \begin{cases} \dfrac{E_{f2} n_{2_{i,c}} R_{f2}^4}{2 E_{f1} R_{i,c}^2 \ln\left(R_t / R_{i,c}\right) \left(R_{f1}^2 V_{f2} + R_{f2}^2 V_{f1}\right)} & \text{for } \alpha = 2 \\[2ex] \dfrac{E_{f2} n_{2_{i,c}} R_{f2}^4 R_{i,c}^{-\alpha} (\alpha - 2)}{2 E_{f1} \left(\left(R_{f1}^2 V_{f2} + R_{f2}^2 V_{f1}\right) \left(R_{i,c}^2 \left(1/R_{i,c}\right)^\alpha - R_t^2 \left(1/R_t\right)^\alpha\right)\right)} & \text{otherwise.} \end{cases}
\end{aligned} \tag{10}$$

The model is very powerful as it takes into account the cluster size, RVE size, volume fractions, fibre radius and elastic properties of each fibre population with simple analytical equations. Moreover, it can represent different matrix behaviours or effects not present into the model by adjusting the value of α.

As there can be multiple clusters along the RVE, a superposition rule is considered. Therefore, the total *SCF* for an intact fibre element is obtained by linear superposition of the *SCF* of all clusters. Nonetheless, the *SCF* of a given element is bounded according to shear-lag transfer. This limitation ensures that there is a stress continuity between elements inside any ineffective length (elements where $0 < D_{p,q} < 1$) that are not affected by *SCF*, and subsequent intact elements ($D_{p,q} = 0$), which can be affected by the *SCF*. Thus, the total *SCF* of an intact element p, q is given by

$$SCF_{p,q} = \begin{cases} \min\left(SCF^0_{p,q}, SCF^L_{p,q}\right) & \forall p, q : D_{p,q} = 0 \\ 1 & \text{otherwise,} \end{cases} \tag{11}$$

where $SCF^0_{p,q}$ is the *SCF* predicted by the linear superposition of the contribution of all clusters using the previous δ and λ functions given by

$$\begin{aligned} SCF^0_{p,q} &= 1 + \sum_{i=1}^{N_p} \sum_{c=1}^{N_i^c} \delta_{11_{(q-c)}} \lambda_{1_{(p-i)}} + \delta_{12_{(q-c)}} \lambda_{2_{(p-i)}} \quad \forall i, c : n_{i,c} > 0 \quad \& \quad q \in f1 \\ SCF^0_{p,q} &= 1 + \sum_{i=1}^{N_p} \sum_{c=1}^{N_i^c} \delta_{22_{(q-c)}} \lambda_{2_{(p-i)}} + \delta_{21_{(q-c)}} \lambda_{1_{(p-i)}} \quad \forall i, c : n_{i,c} > 0 \quad \& \quad q \in f2 \end{aligned} \tag{12}$$

where f_1 and f_2 are fibre populations 1 and 2 respectively. $SCF^L_{p,q}$ is the *SCF* limitation for broken fibre q to achieve stress continuity. This limit for intact element p, q is calculated according to the slope of the stress gradient of the nearest ineffective length, $1/L^{\text{in}}_{i,q}$, in the fibre q, multiplied by the distance between planes i and p:

$$SCF^L_{p,q} = \min\left(\frac{1}{L^{\text{in}}_{i,q}} |i - p|\, l\right) \quad \forall i : D_{i,q} = 1 \tag{13}$$

It should be noted that the broken and damaged fibre elements are not excluded from Eq. (8). Therefore, the *SCF* of each intact element is computed independently of the percentage of broken and damaged elements. However, the percentage of broken and damaged elements is taken into account to compute the strain of each plane, ε_p, and the stress ratio, Ω_p, which affect the final stress of the elements, $\sigma_{p,q}$. This is explained in detail in Guerrero *et al.* [2].

3. Methodology

In a hybrid composite the stress redistribution around broken fibres depends mainly on the elastic and geometrical properties of both fibres, the matrix behaviour (plastic or elastic), the hybrid volume fraction as well as the local fibre arrangement [10, 11]. All these properties will affect the creation and propagation of clusters that lead to final failure. In this work, the effects of the Young's modulus of the fibres, matrix shear strength (plastic or elastic) and hybrid volume fraction on the stress redistribution around a broken fibre are investigated in detail. Later, their effect on the tensile failure behaviour are also evaluated. The simulations are performed with the PFM using the new *SCF* model presented in previous section 2.1.3. All simulations are compared with the SEM [24] to validate the results.

A modified version of Melro's *et al.* [35] random fibre generator is used to create a RVE of width, thickness and length of $75 \times 75 \times 300$ times the fibre radius. The element length is always 2 times the fibre radius, with both fibres in the RVE having the same radius. The same RVE is used for both PFM and SEM when studying the same problem. Note however that a new RVE is generated for each case in study. To observe the differences in load redistribution and failure process with different properties, three hybrid composites are considered by combining different fibres. These hybrids correspond to AS4-Eglass, M50S-AS4 and AS4-T800G, whose properties are shown in Table 1. In all cases, the matrix corresponds to epoxy with elastic properties $E_{\mathrm{m}} = 1260$ MPa and $G_{\mathrm{m}} = 450$ MPa. To understand the impact of the matrix behaviour, all cases are simulated with plastic ($\tau_q = 50$ MPa) and elastic matrix ($\tau_q \to \infty$). In addition, each hybrid is simulated with a hybrid volume fraction of 25%, 50% and 75%. Here, the Hybrid Volume Fraction (*HVF*) is referred to be as the percentage of HE fibre volume fraction, V_{HE}, over the total fibre volume fraction, $HVF = (V_{\mathrm{HE}}/V_{\mathrm{f}}) \cdot 100$.

In the case of SEM, the model calculates all unknown variables directly from the equilibrium equations, as a function of the material properties and RVE geometry, being a very robust tool. However, it is less efficient computationally than the PFM. For the PFM instead, the ineffective length and *SCF* need to be applied according to the matrix behaviour. In all cases where the matrix is plastic ($\tau_q \neq \infty$), the ineffective length and damage are simulated within equations (2) and (3). In these cases, the *SCF* is calculated using $\alpha = 2$. However, when the matrix is elastic ($\tau_q = \infty$), then the ineffective length and damage are simulated with equations (4) and (5) and $\alpha = 3.8$. It is worth mentioning that, when the matrix is plastic, its behaviour is considered to be perfectly plastic in the PFM, whilst it is elastic-plastic in the SEM.

To investigate the stress redistribution around breaks, a broken fibre is arbitrarily placed around the middle of the RVE for each hybrid composite. This broken fibre is either the fibre with lower Young's modulus (LM) or the fibre with higher Young's modulus (HM). Usually, the LM fibre corresponds to the fibre with larger failure strain, i.e. the HE fibre, whereas the HM fibre corresponds to the fibre with smaller failure strain, i.e. the LE fibre. Even tough the LE fibres will break before the HE fibres, it is important to study the HE fibre load redistribution as well as towards final failure the HE fibre also fails. A remote tensile strain, ε, of 2% is applied and the consequent obtained load redistribution around the broken fibre is characterized with three different metrics. The first one is the maximum *SCF* obtained on intact LM and HM fibres. The *SCF* is calculated as the ratio between the actual stress on the fibre over the stress if there were no breaks, i.e. $E_f\varepsilon$. The second metric is the ineffective length of the broken fibre, which is defined as the distance where the broken fibre recovers 90% of the nominal load, whereas the last metric is the radial influence length. This is defined as the maximum distance in the break plane in which the *SCF* is higher than 1%. The results shown for both the ineffective length and radial length are normalised by the fibre radius. Ten realisations are performed for each case, leading to a total of 360 simulations.

To understand the influence of the modelling parameters on the tensile failure process, the same hybrid composites are simulated under fibre tensile loading. Moreover, non-hybrid composites of each fibre type are also simulated. To do so, a random strength, $\sigma^{\mathrm{ult}}_{p,q}$, is generated for each element in the RVE according to the Weibull distribution [36] with $P_{p,q} = 1 - \exp\left(-(l/L_0)\left(\sigma^{\mathrm{ult}}_{p,q}/\sigma_0\right)^m\right)$, where $P_{p,q}$ is a random number between 0 and 1, while σ_0, L_0 and m are the corresponding Weibull parameters of the fibre element shown in Table 1. To compare the results between simulations, different metrics are proposed based on literature [37]. The first metric is the yield stress, σ^{y}, which is understood as the knee point where the stress-strain curve deviates from the initial linear elastic regime at a strain of 0.1%. The second metric is the ductile strain, ε^{d}, defined as the strain difference between the strain at peak stress, and the initial slope line at the failure stress level $\left(\varepsilon^{\mathrm{d}} = \varepsilon^{\mathrm{ult}} - \sigma^{\mathrm{ult}}/E_0\right)$, where E_0 is the initial Young's modulus of the composite given by the rule of mixtures. The third metric is the peak stress, σ^{ult}, whereas the fourth metric is the strain at peak stress, $\varepsilon^{\mathrm{ult}}$. These metrics are summarized in Figure 2. The fifth metric is the cluster size at peak stress, N^{c}. Here, two broken fibres belong to the same cluster if the distance between centres is smaller than 4 times the fibre radius and the axial distance between break planes is smaller than 10 times the fibre radius [3, 20, 24]. It should be noted that the definition of clusters used to assess the damage evolution explained in this section, is different than the one used for calculating the *SCF* and ineffective length shown in previous Section 2.1.2. This is done to allow a fair comparison between the analytical and numerical model, and other models in the literature. The sixth and final metric is the fibre break density at peak stress, $\delta_{\mathrm{f}}^{\mathrm{ult}}$. Five realisations are performed for each case in study, leading to 110 simulations in total.

4. Stress redistribution around breaks

In this section the stress redistribution around a broken fibre is analysed. A comparison of the results between the SEM and the analytical *SCF* model used in the framework of the PFM is performed to asses the validity of the analytical model. The overall volume fraction considered was 60% for all cases studied. It should be noted that in this section, because the fibres have no strength, the *HVF* is referred to be as the percentage of LM fibre volume fraction over the total fibre volume fraction.

4.1. Stress concentration factor

The trends predicted by both PFM and SEM are the same for all hybrid materials and matrix behaviour, even though the absolute values are not the same. However, their relative difference is remarkably small considering the simplicity of the analytical model. These results justify the assumption done in Eq. 9.

In Figure 3, the *SCF* around a broken HM fibre is shown with a plastic matrix and an elastic matrix as a function of the *HVF* for the different hybrids in study. The *SCF* calculated is larger for the LM fibres when compared with the HM fibres. As the LM fibres have a lower stiffness, their stress before the break was lower compared with the

HM fibre. Hence, the relative increase of stress is larger on the LM fibre causing a larger *SCF* [10].

Interestingly, the *SCF* on HM fibres decreases when adding LM fibres, while the opposite happens for the *SCF* on LM fibres. That should be related to the fact that by increasing the LM fibre content, the distance of the HM fibre to the break increases, and the load to redistribute is mainly taken by the LM fibres. This will cause larger hybrid effects at smaller HM volume fractions as has already been reported in literature [2, 11, 12, 18]. Moreover, the *SCF* on HM fibres is not strongly affected by the LM stiffness, whereas the opposite happens with the *SCF* on LM fibres. The larger the ratio between the stiffness of the HM and LM fibre is, the larger is the *SCF* obtained on the LM fibres. This fact agrees well with the findings of Swolfs *et al.* [10].

The matrix behaviour i.e. plastic or elastic changes the maximum value of *SCF*, being larger with elastic matrix, however, the trends are the same. The reason for this difference is the fact that, in an elastic matrix, there is no upper limit for shear stress transfer between fibre and matrix, hence causing a more localised effect and larger *SCF*.

In Figure 4 the *SCF* around a broken LM fibre is shown with both plastic and elastic matrix for different *HVF* and materials. The *SCF* on HM fibres again decreases by increasing the content of LM fibres, whilst the opposite happens with the LM fibres. Interestingly, the *SCF* on both HM and LM fibres are smaller than in the previous case. That is related to the fact that the LM fibre carried less load than the HM fibre before failure, hence resulting in smaller *SCF*. It should be noted however, that in reality the LM fibres usually fail after the failure of multiple HM fibres. Thus, the *SCF* obtained will be much larger than the ones predicted here, as the HM fibres no longer support load. The *SCF* on the LM fibre is not strongly affected by the stiffness of the HM fibre. Nonetheless, the *SCF* on the HM fibre is highly influenced by the stiffness of the LM fibre. A smaller stiffness ratio between HM and LM fibre leads to a larger *SCF* on the HM fibres, which is the opposite as observed in the previous case.

Although the models are able to take into account fibres with different radii [2, 24], in this study the fibres were considered to always have the same radii. Otherwise, it would add another layer of complexity due to higher differences in the microstructures of the composites analysed.

4.2. *Ineffective length*

In Figure 5 the ineffective length is shown for a broken HM fibre and a broken LM fibre with both plastic and elastic matrix as a function of the *HVF* for each material system.

The ineffective length is larger for the HM fibre than for the LM fibre. That is due to its stiffness: a larger stiffness means that a larger load needs to be recovered, hence causing a larger ineffective length. Interestingly, the ineffective length is not significantly affected by the stiffness of the other fibre in the hybrid, which corresponds well to the findings of Swolfs *et al.* [10]. Similarly, the *HVF* has a small effect on the ineffective length. In Figure 5 d), a minimum can be observed for the SEM at $HVF = 50\%$, however, the difference is small compared to other volume fractions. In the same way, in Figure 5 b) and c) a small increase of ineffective length is observed in the SEM for $HVF = 75\%$. In any of these cases, the small difference in ineffective length due to the *HVF* should be related to the changes in the microstructure, as the ratio between HM and LM fibres is different.

The ineffective length exhibits a large change between plastic and elastic matrix, the same trend that was observed for the *SCF*. The ineffective length is smaller for an elastic matrix, as there is no limit in shear stress transfer, making it possible for the stress to be recovered in the broken fibre in a shorter region. With the plastic matrix the shear transfer is limited by the matrix shear strength resulting in a larger ineffective length. In any case the trends remain the same for both matrix behaviours.

In general, the results predicted between the SEM and the analytical models in PFM follow similar trends, although some differences are observed. In the PFM the ineffective length is always smaller than in SEM. This is specially evident for the plastic matrix cases. There are two main reasons which can explain this difference. Firstly, with a plastic matrix, the behaviour of the matrix is elastic-plastic in the SEM, whilst it is perfectly plastic in PFM. Because of this, the shear stress is constant along the ineffective length, causing an underprediction of the ineffective length. This issue could in principle be improved by using an elastic-plastic model in PFM instead of a perfectly plastic. The second reason could be related to the microstructure. In the SEM, the ineffective length of each broken fibre depends on the local stiffness around the broken fibre. This means that if the broken fibre is surrounded by more LM fibres (with lower stiffness), then the ineffective length of the broken fibre is higher. This explains why the SEM predicts an increase in ineffective length at larger *HVF*. However, this effect is unlikely to be captured by a simple analytical model.

4.3. Radial influence length

The radial influence length for each material system, as a function of the *HVF* is shown in Figure 6.

As it can be observed, the radial influence length is larger when a HM fibre is broken than when a LM fibre is. That is because the HM fibre has a larger stiffness, causing a larger load to be redistributed over intact fibres leading to a larger radial length. In most cases a small increase of the radial length can be observed by increasing the *HVF*. This increase is larger for the SEM than for the PFM, although overall the trends are similar. In general, the radial influence length is slightly larger for the PFM than for SEM.

Overall the radial length is affected by the stiffness of the fibres. A larger ratio of stiffness between HM and LM fibres causes a larger radial influence length when the HM fibre is broken. The opposite trend is observed when the LM fibre is broken. This observation corresponds well to what was observed with the *SCF*.

Changing the matrix from elastic to plastic maintains the same trends as it was seen with the *SCF* and ineffective length. As expected, the radial length is smaller with an elastic matrix, which is again caused by the no upper limit in shear transfer between fibre and matrix. In any case, the radial influence length is heavily dependent on the microstructure and its average value for each realization performed presents an error of approximately ±1 mm/mm.

5. Tensile behaviour

In this section the tensile failure of the hybrid materials cases used in Section 4 is simulated under strain controlled conditions. A comparison of results is performed between SEM and PFM. In this section, the total fibre volume fraction considered is 50%.

A summary of all the results obtained for the hybrid materials with plastic matrix is presented in Table 2, while the results with elastic matrix are shown in Table 3. The results for the non-hybrid cases are summarized in Table 4. The presented results, correspond to the average of 5 realisations for each case. The average computational time for performing one run of the cases studied was 1314 s for the SEM, whereas it was 114 s for the PFM. Therefore, the simplified model is approximately 10 times faster.

The stress-strain curves obtained for all materials with a plastic matrix are shown in Figure 7. The tensile behaviour predicted by the two modelling approaches is in good agreement for all cases despite of the differences in the modelling assumptions. In general, the PFM overpredicts the final failure of the composite, leading to larger peak stresses, yield stresses, strain and break densities, when compared with the SEM.

The failure process is seen to be very different for each hybrid configuration and varies greatly with the *HVF*. For the AS4-Eglass hybrid, no ductility is observed at the different *HVF* simulated. However, at a $HVF = 75\%$, there is a larger stiffness loss when compared with $HVF = 50\%$ and $HVF = 25\%$ before the final load drop, which suggests that ductility could be present for $HVF > 75\%$. This is also indicated by the fibre break density evolution presented in Figure 8. As it can be seen, the fibre break density increases exponentially for all hybrid volume fractions leading to a brittle failure, nonetheless, this increase is less abrupt for $HVF = 75\%$.

For the M50S-AS4 hybrid, brittle failures are also obtained at *HVF* of 25% and 50%. Nonetheless, a rather large ductility of around 0.5% is predicted by the models for *HVF*=75%, meaning that for this composite material the failure process is gradual. This is clearly demonstrated by the evolution of fibre break density, which increases linearly but not exponentially, until final failure.

Similarly, a ductility of around 0.7% is observed within the AS4-T800G hybridization at a $HVF = 75\%$. However, by decreasing the *HVF* brittle failures are obtained. In the case of $HVF = 25\%$, the failure is completely brittle whereas for the $HVF = 50\%$ two load drops can be observed. The first load drop corresponds to the failure of the LE fibres, whilst the second one corresponds to the failure of the HE fibres. Nevertheless this case cannot be considered as ductile because the failure is not really continuous.

In general, the predicted cluster size is larger for the PFM than for SEM. The reason for this is likely to be related to the fact that final failure occurs later in PFM. In any case, the cluster size predicted are in general in good agreement with results of non-hybrid composites [3]. Similarly, the fibre break density is in general larger for the PFM for the same reason, although in this case both models predict larger values than seen in the literature [3]. The fibre break density seems to increase with ductility. The larger is the ductile strain, the larger is the break density. This is caused by the fact that final failure is being delayed, leading to larger break densities. For the M50S-AS4 hybrid, the fibre break density at maximum stress for $HVF = 75\%$ is more than 2 times larger compared to $HVF = 25\%$, being this increase from 4235 to 9692 mm^{-3} for SEM and from 7063 to 16229 mm^{-3} for PFM. Similarly, for the AS4-T800G hybrid, the fibre break density at $HVF = 75\%$ is approximately 3 times larger than at $HVF = 25\%$, with an increase from 3831 to 10670 mm^{-3} and 6397 to 21340 mm^{-3} for SEM and PFM respectively. It is worth mentioning that both the cluster size and fibre break density are here being compared with results of non-hybrid composites, which are brittle and less damage tolerant than the analysed hybrids. Therefore, this comparison should be taken with care. Nonetheless, although there is no certainty in the results for hybrid composites, the models seem to partially capture the results in non hybrid composites and their application to hybrid composites, although debatable, can lead to important insights.

The predicted stress-strain curves using an elastic matrix are shown in Figure 9, while the fibre break density can be seen in Figure 10. Both models are again in good agreement for most material configurations, although now the PFM is in general underpredicting final failure compared to SEM. Nonetheless, the obtained stress-strain curves and failure process differ greatly from the ones observed by using a plastic matrix. Unlike the plastic matrix case, some ductility appears within the AS4-Eglass hybrid at a $HVF = 75\%$. However, a very small ductility is predicted for the M50S-AS4 hybrid at a $HVF = 75\%$ compared to the plastic matrix case. The differences between plastic and elastic matrix are even larger for the AS4-T800G hybrid. With this material, the ductile strain at a $HVF = 75\%$ is of 1%, which is much larger than the 0.7% predicted for plastic matrix. Similarly, at a $HVF = 50\%$ a large ductility of 1.5% for SEM and 0.5% for PFM is predicted whilst no ductility was present with a plastic matrix.

By further analysing the cluster evolution and break density with an elastic matrix, larger differences appear in comparison with the plastic matrix. For the ductile cases, the models with an elastic matrix predict a much larger break density than with a plastic matrix. The cluster size is also unrealistically large compared with experimental data [3].

This is especially evident for the AS4-T800G hybrid, in which the cluster size predicted by the models exceeds the number of fibres in the RVE for $HVF = 75\%$ and $HVF = 50\%$. This means that in some cases, some fibres were broken more than once over the 10 axial element lengths considered, corresponding to 20 times the fibre radius. Therefore, the same fibre was broken multiple times in the same cluster. This effect is even more exaggerated due to the small Weibull modulus, m, of the T800G fibre which causes a large strength variation for that fibre. However, it should be highlighted again that both the cluster size and fibre-break density are being compared with results of non-hybrid composites which are brittle and less damage tolerant than the simulated hybrids.

For the cases of the non-hybrid composites the models are again in good agreement. For these materials the final failure is brittle for all cases, being similar between elastic and plastic matrix. However, the fibre break density and cluster size are again very large for some cases with elastic matrix and do not correspond well to data available in the literature [3].

The large differences of results between plastic and elastic matrix highlight that the differences in load redistribution, seen in previous Section 4, lead to very different failure progression. In an elastic matrix, the shear stress transfer between fibre and matrix is not limited which causes the stress redistribution to be always very localized around the break. As a consequence, many isolated clusters along the model appear which need to grow very large in size to propagate unstably. This is the reason why the cluster size is usually larger for the elastic matrix cases. Similarly, it should also explain why larger ductilities are observed with an elastic matrix. In a real composite however, the shear stresses are limited by the matrix strength, like it is the case with a plastic matrix approach. Results of this work suggest that, while an elastic matrix may lead to similar failure prediction in non-hybrid composites compared to a plastic matrix, the use of an elastic matrix can lead to inaccurate results when modelling hybrid composites. Nonetheless, it is impossible to further validate the results due to the lack of experimental data. Furthermore, a better definition of cluster size is needed to avoid clusters larger than the number of fibres.

6. Conclusions

In this work, a new analytical model for predicting the *SCF* around clusters of broken fibres in hybrid unidirectional composites was presented. The model was used within the framework of a PFM [2] to study the stress redistribution around breaks in different hybrid composites and their effect on the tensile response and failure process. The results were validated by comparing with the SEM [24].

The predicted stress redistribution around broken fibres in hybrid composites was seen to vary with the stiffness ratio of the fibres on the hybrid, the matrix behaviour being plastic or elastic, the broken fibre stiffness as well as the hybrid volume fraction. Three different metrics were used to quantify this load redistribution: maximum *SCF* on HM and LM fibres, ineffective length and radial length.

The *SCF* on an intact fibre with different stiffness than the broken fibre is affected by the stiffness ratio of both fibres. The larger the ratio, the larger the *SCF* when the HM fibre is broken, whereas the opposite happens when the LM fibre is broken. Adding LM fibres into the hybrid composite decreases the *SCF* on HM fibres, which should lead to larger hybrid effects. When a HM fibre is broken, the *SCF* is larger on the LM fibres than on the HM fibres. However, the *SCFs* are smaller in both populations when the LM fibre is broken. Changing the matrix from plastic to elastic has an important impact on the *SCF*. With an elastic matrix, the *SCF* is larger due to the fact that there is no limit in shear stress transfer. The new proposed analytical model predicted well the trends and stress redistribution in all cases and is in good agreement with the SEM. Moreover, assuming that the overload carried by an intact fibre due to a break does not depend on its Young's modulus and radius, provides a good correlation between the analytical model and the SEM.

The ineffective length was found to depend mainly on the stiffness of the broken fibre. The larger the stiffness, the larger the ineffective length. As a difference from the *SCF*, the stiffness of the hybridization fibre and the *HVF* has no significant impact on the ineffective length. However, the matrix behaviour has a strong effect, being the ineffective length smaller with an elastic matrix. Finally, the radial influence length follows the same trends as the *SCF* and is smaller with an elastic matrix.

In addition, a simulation of the fibre tensile failure of different hybrid materials was performed under strain controlled conditions. Different ductile responses were predicted for some composites at low *HVF*, whereas in other cases brittle and sudden failures were obtained. The ductile composites presented a gradual and progressive increase of fibre break density, whereas an exponential increase was obtained for the brittle materials.

Large differences were again found between plastic and elastic matrix, meaning that the differences in load redistribution lead to different failure progression. When the matrix was considered elastic, many isolated clusters appeared along the model. These clusters needed to grow very large in size before unstable propagation. As a consequence, unrealistically large cluster size and break densities were predicted for some simulations. This wasn't the case with a plastic matrix, which presented more realistic results compared to experiments [3]. Therefore, results suggest that using an elastic matrix may lead to erroneous predictions when modelling hybrid composites. Additional experimental data is required to further validate and improve the different models for hybrid composites.

Acknowledgments

The authors of Universitat de Girona acknowledge the financial support from the Spanish Ministerio de Economía, Industria y Competitividad (MINECO) under the projects MAT2015-69491-C3-1-R and TRA2015-71491-R co-financed by the European Regional Development Fund (ERDF). Jose M. Guerrero acknowledges the predoctoral Grant BES-2016-078270 from the Subprograma Estatal de Formación del MICINN cofinanced by the European Social Fund. Rodrigo P. Tavares acknowledges the support of the Portuguese Government's Fundação para a Ciência e Tecnologia, under the Grant SFRH/BD/115872/2016. Fermin Otero acknowledges the funding of Project NORTE-01-0145-FEDER-000022 SciTech Science and Technology for Competitive and Sustainable Industries, cofinanced by Programa Operacional Regional do Norte (NORTE2020), through ERDF. Pedro P. Camanho acknowledges the funding of Project PTDC/EMS-PRO/4732/2014, cofinanced by Programa Operacional Competitividade e Internacionalização and Programa Operacional Regional de Lisboa, through ERDF and by National Funds through FCT - Fundação para a Ciência e Tecnologia.

Data availability

The raw/processed data required to reproduce these findings cannot be shared at this time due to legal or ethical reasons.

References

[1] A. Turon, J. Costa, P. Maimí, D. Trias, J. A. Mayugo, A progressive damage model for unidirectional fibre-reinforced composites based on fibre fragmentation. Part I: Formulation, Composites Science and Technology 65 (13) (2005) 2039–2048. doi:10.1016/j.compscitech.2005.04.012.

[2] J. Guerrero, J. Mayugo, J. Costa, A. Turon, A 3D Progressive Failure Model for predicting pseudo-ductility in hybrid unidirectional composite materials under fibre tensile loading, Composites Part A: Applied Science and Manufacturing 107 (2018) 579–591. doi:10.1016/j.compositesa.2018.02.005.

[3] Y. Swolfs, H. Morton, A. E. Scott, L. Gorbatikh, P. A. S. Reed, I. Sinclair, S. M. Spearing, I. Verpoest, Synchrotron radiation computed tomography for experimental validation of a tensile strength model for unidirectional fibre-reinforced composites, Composites Part A: Applied Science and Manufacturing 77 (2015) 106–113. doi:10.1016/j.compositesa.2015.06.018.

[4] A. Bunsell, L. Gorbatikh, H. Morton, S. Pimenta, I. Sinclair, M. Spearing, Y. Swolfs, A. Thionnet, Benchmarking of strength models for unidirectional composites under longitudinal tension, Composites Part A: Applied Science and Manufacturing 111 (June 2017) (2018) 138–150. doi:10.1016/j.compositesa.2018.03.016.

[5] A. E. Scott, M. Mavrogordato, P. Wright, I. Sinclair, S. M. Spearing, In situ fibre fracture measurement in carbon-epoxy laminates using high resolution computed tomography, Composites Science and Technology 71 (12) (2011) 1471–1477. doi:10.1016/j.compscitech.2011.06.004.

[6] G. Czél, M. R. Wisnom, Demonstration of pseudo-ductility in high performance glass/epoxy composites by hybridisation with thin-ply carbon prepreg, Composites

Part A: Applied Science and Manufacturing 52 (2013) 23–30. doi:10.1016/j.compositesa.2013.04.006.

[7] G. Czél, M. Jalalvand, M. R. Wisnom, Design and characterisation of advanced pseudo-ductile unidirectional thin-ply carbon/epoxy-glass/epoxy hybrid composites, Composite Structures 143 (2016) 362–370. doi:10.1016/j.compstruct.2016.02.010.

[8] Y. Swolfs, L. Gorbatikh, I. Verpoest, Fibre hybridisation in polymer composites: A review, Composites Part A: Applied Science and Manufacturing 67 (2014) 181–200. doi:10.1016/j.compositesa.2014.08.027.

[9] J. Xing, G. Hsiao, T.-W. Chou, A Dynamic Explanation of The Hybrid Effect, Journal of Composite Materials 15 (5) (1981) 443–461. doi:10.1177/002199838101500504.

[10] Y. Swolfs, L. Gorbatikh, I. Verpoest, Stress concentrations in hybrid unidirectional fibre-reinforced composites with random fibre packings, Composites Science and Technology 85 (2013) 10–16. doi:10.1016/j.compscitech.2013.05.013.

[11] Y. Swolfs, I. Verpoest, L. Gorbatikh, Maximising the hybrid effect in unidirectional hybrid composites, Materials and Design 93 (2016) 39–45. doi:10.1016/j.matdes.2015.12.137.

[12] Y. Swolfs, R. M. McMeeking, I. Verpoest, L. Gorbatikh, The effect of fibre dispersion on initial failure strain and cluster development in unidirectional carbon/glass hybrid composites, Composites Part A: Applied Science and Manufacturing 69 (2014) 279–287. doi:10.1016/j.compositesa.2014.12.001.

[13] M. R. Wisnom, G. Czel, Y. Swolfs, M. Jalalvand, L. Gorbatikh, I. Verpoest, Hybrid effects in thin ply carbon/glass unidirectional laminates: Accurate experimental determination and prediction, Composites Part A: Applied Science and Manufacturing 88 (2016) 131–139. doi:10.1016/j.compositesa.2016.04.014.

[14] J. D. Vanegas-Jaramillo, A. Turon, J. Costa, L. J. Cruz, J. A. Mayugo, Analytical model for predicting the tensile strength of unidirectional composites based on the

density of fiber breaks, Composites Part B: Engineering 141 (February 2017) (2018) 84–91. doi:10.1016/j.compositesb.2017.12.012.

[15] C. Y. Hui, S. L. Phoenix, M. Ibnabdeljalil, R. L. Smith, An exact closed form solution for fragmentation of Weibull fibers in a single filament composite with applications to fiber-reinforced ceramics, Journal of the Mechanics and Physics of Solids 43 (10) (1995) 1551–1585. doi:10.1016/0022-5096(95)00045-K.

[16] W. A. Curtin, Exact theory of fibre fragmentation in a single-filament composite, Journal of Materials Science 26 (19) (1991) 5239–5253. doi:10.1007/BF01143218.

[17] J. M. Neumeister, A constitutive law for continuous fiber reinforced brittle matrix composites with fiber fragmentation and stress recovery, Journal of the Mechanics and Physics of Solids 41 (8) (1993) 1383–1404. doi:10.1016/0022-5096(93)90085-T.

[18] R. P. Tavares, A. R. Melro, M. A. Bessa, A. Turon, W. K. Liu, P. P. Camanho, Mechanics of hybrid polymer composites: analytical and computational study, Computational Mechanics 57 (3) (2016) 405–421. doi:10.1007/s00466-015-1252-0.

[19] Y. Swolfs, R. M. McMeeking, V. P. Rajan, F. W. Zok, I. Verpoest, L. Gorbatikh, Global load-sharing model for unidirectional hybrid fibre-reinforced composites, Journal of the Mechanics and Physics of Solids 84 (2015) 380–394. doi:10.1016/j.jmps.2015.08.009.

[20] R. P. Tavares, J. M. Guerrero, F. Otero, A. Turon, J. A. Mayugo, J. Costa, P. P. Camanho, Effects of local stress fields around broken fibres on the longitudinal failure of composite materials, International Journal of Solids and Structures. In press.doi:10.1016/j.ijsolstr.2018.08.027.

[21] S. Pimenta, A computationally-efficient hierarchical scaling law to predict damage accumulation in composite fibre-bundles, Composites Science and Technology 146 (2017) 210–225. doi:10.1016/j.compscitech.2017.04.018.

[22] L. St-Pierre, N. J. Martorell, S. T. Pinho, Stress redistribution around clusters of broken fibres in a composite, Composite Structures 168 (2017) 226–233. doi:10.1016/j.compstruct.2017.01.084.

[23] S. Pimenta, S. T. Pinho, Hierarchical scaling law for the strength of composite fibre bundles, Journal of the Mechanics and Physics of Solids 61 (6) (2013) 1337–1356. doi:10.1016/j.jmps.2013.02.004.

[24] R. P. Tavares, F. Otero, A. Turon, P. P. Camanho, Effective simulation of the mechanics of longitudinal tensile failure of unidirectional polymer composites, International Journal of Fracture 208 (1-2) (2017) 269–285. doi:10.1007/s10704-017-0252-9.

[25] T. Okabe, H. Sekine, K. Ishii, M. Nishikawa, N. Takeda, Numerical method for failure simulation of unidirectional fiber-reinforced composites with spring element model, Composites Science and Technology 65 (6) (2005) 921–933. doi:10.1016/j.compscitech.2004.10.030.

[26] T. Okabe, N. Takeda, Y. Kamoshida, M. Shimizu, W. A. Curtin, A 3D shear-lag model considering micro-damage and statistical strength prediction of unidirectional fiber-reinforced composites, Composites Science and Technology 61 (12) (2001) 1773–1787. doi:10.1016/S0266-3538(01)00079-3.

[27] L. Mishnaevsky, P. Brøndsted, Micromechanisms of damage in unidirectional fiber reinforced composites: 3D computational analysis, Composites Science and Technology 69 (7-8) (2009) 1036–1044. doi:10.1016/j.compscitech.2009.01.022.

[28] A. Thionnet, H. Y. Chou, A. Bunsell, Fibre break processes in unidirectional composites, Composites Part A: Applied Science and Manufacturing 65 (2014) 148–160. doi:10.1016/j.compositesa.2014.06.009.

[29] T. Okabe, K. Ishii, M. Nishikawa, N. Takeda, Prediction of Tensile Strength of Unidirectional CFRP Composites, Advanced Composite Materials 19 (3) (2010) 229–241. doi:10.6089/jscm.33.205.

[30] Kelly A., W. Tyson, Tensile properties of fibre-reinforced and metals: copper/tungsten and copper/molybdenum, Journal of the mechanics and physics of solids 13 (6) (1965) 329–350. doi:10.1016/0022-5096(65)90035-9.

[31] H. Cox, The elasticity and strength of paper and other fibrous materials, British Journal of Applied Physics 3 (3) (1952) 72–79. doi:10.1088/0508-3443/3/3/302.

[32] C. M. Landis, R. M. McMeeking, A shear-lag model for a broken fiber embedded in a composite with a ductile matrix, Composites Science and Technology 59 (3) (1999) 447–457. doi:10.1016/S0266-3538(98)00091-8.

[33] A. Eitan, H. D. Wagner, Fiber interactions in two-dimensional composites, Applied Physics Letters 58 (10) (1991) 1033–1035. doi:10.1063/1.105209.

[34] X. F. Zhou, H. D. Wagner, Stress concentrations caused by fiber failure in two-dimensional composites, Composites Science and Technology 59 (7) (1999) 1063–1071. doi:10.1016/S0266-3538(98)00145-6.

[35] A. R. Melro, P. P. Camanho, S. T. Pinho, Generation of random distribution of fibres in long-fibre reinforced composites, Composites Science and Technology 68 (9) (2008) 2092–2102. doi:10.1016/j.compscitech.2008.03.013.

[36] W. Weibull, A statistical distribution function of wide applicability, ASME Journal (1952) 293–297.

[37] M. Jalalvand, G. Czél, M. R. Wisnom, Parametric study of failure mechanisms and optimal configurations of pseudo-ductile thin-ply UD hybrid composites, Composites Part A: Applied Science and Manufacturing 74 (2015) 123–131. doi:10.1016/j.compositesa.2015.04.001.

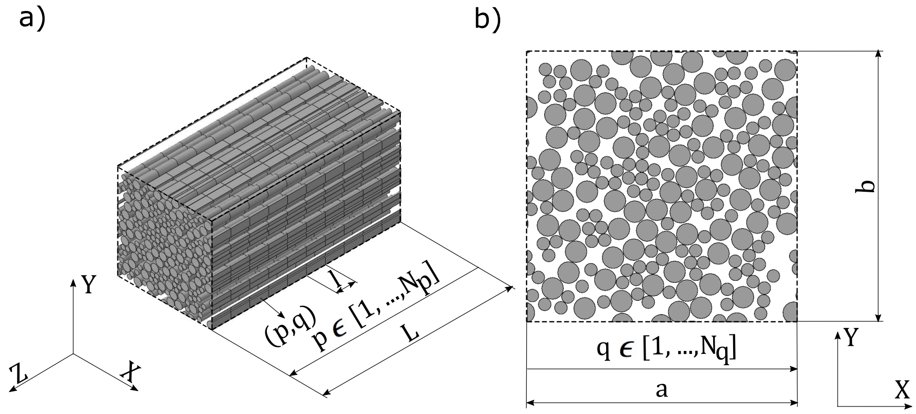

Figure 1: Schema of the RVE used in the PFM: a) 3D view, b) plane view.

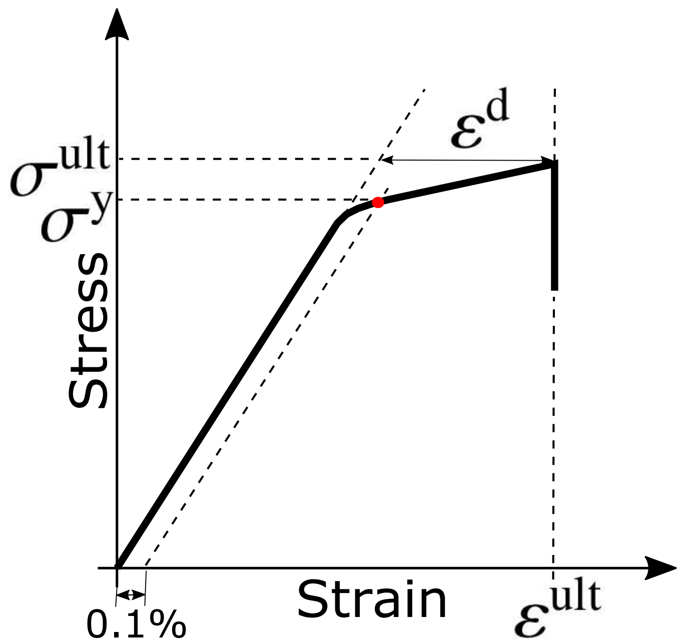

Figure 2: Main metrics used to characterize the tensile behaviour of hybrid composites.

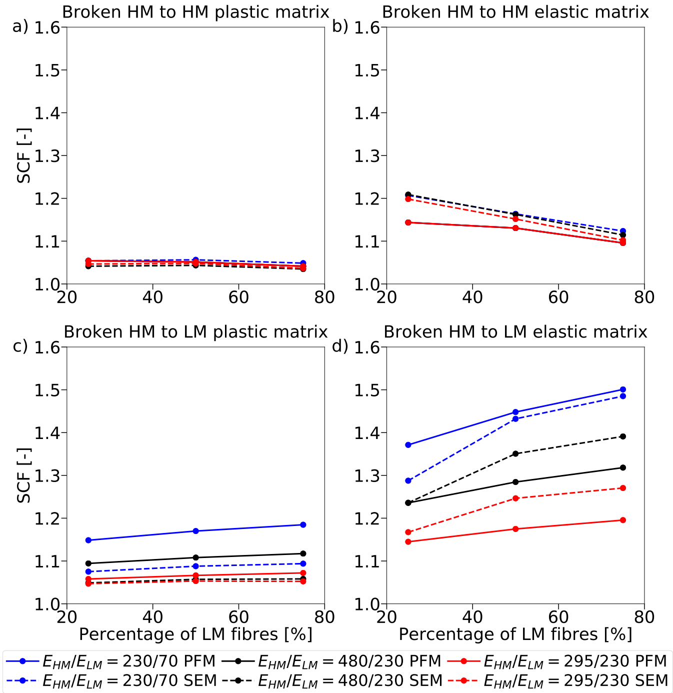

Figure 3: Maximum stress concentration factors around a broken HM fibre as a function of the hybrid volume fraction for different hybridizations: a) on HM fibres with plastic matrix, b) on HM fibres with elastic matrix, c) on LM fibres with plastic matrix, d) on LM fibres with elastic matrix. The average of 10 realisations are shown (τ_q = 50 MPa for plastic matrix). Note that in a) and b), all PFM results are the same.

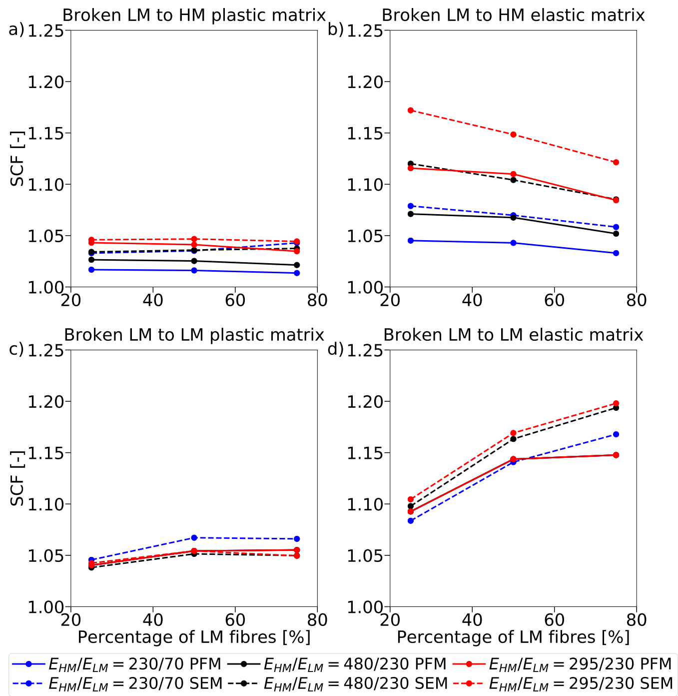

Figure 4: Maximum stress concentration factors around a broken LM fibre as a function of the hybrid volume fraction for different hybridizations: a) on HM fibres with plastic matrix, b) on HM fibres with elastic matrix, c) on LM fibres with plastic matrix, d) on LM fibres with elastic matrix. The average of 10 realisations are shown (τ_q = 50 MPa for plastic matrix). Note that in c) and d), all PFM results are the same.

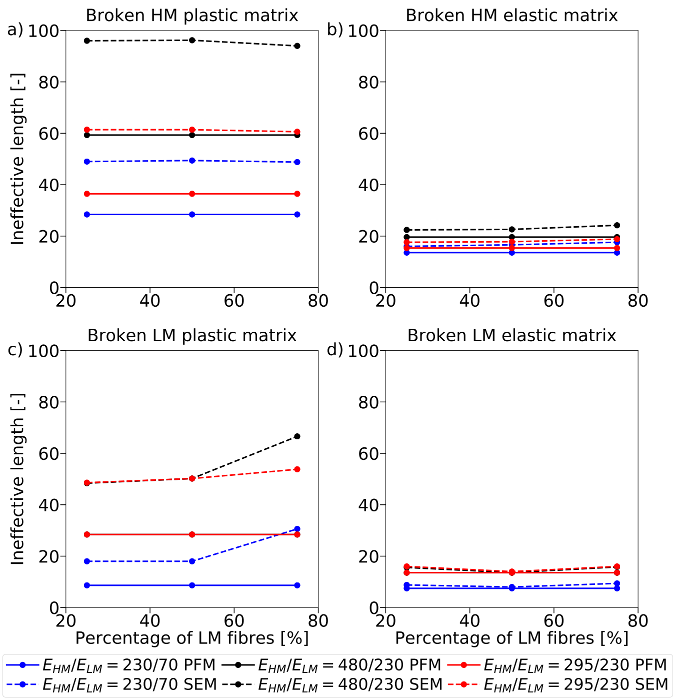

Figure 5: Normalised ineffective length at 90% of load recovery: a) broken HM fibre and plastic matrix, b) broken HM fibre and elastic matrix, c) broken LM fibre and plastic matrix, d) broken LM fibre and elastic matrix. The average of 10 realisations are shown (τ_q = 50 MPa for plastic matrix). Note that in c) and d), the results for $E_{HM}/E_{LM} = 480/230\ PFM$ and $E_{HM}/E_{LM} = 295/230\ PFM$ are the same.

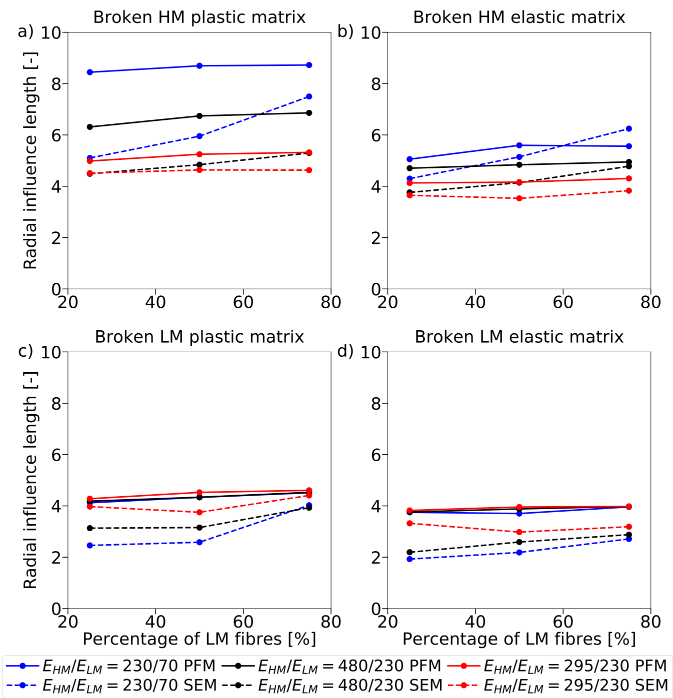

Figure 6: Normalised radial influence length: a) broken HM fibre and plastic matrix, b) broken HM fibre and elastic matrix, c) broken LM fibre and plastic matrix, d) broken LM fibre and elastic matrix. The average of 10 realisations are shown (τ_q = 50 MPa for plastic matrix).

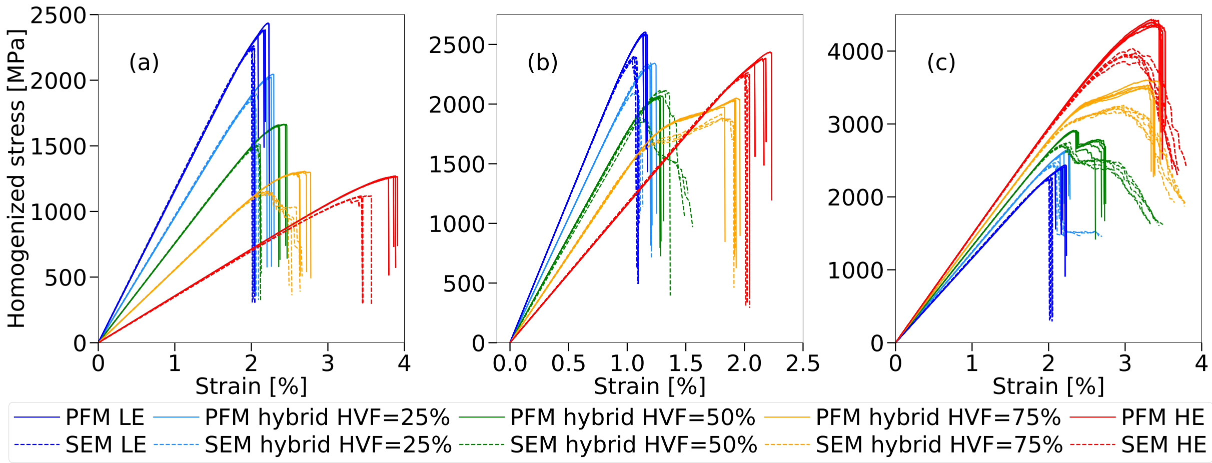

Figure 7: Simulated stress-strain curves for different hybrid materials at different hybrid volume fractions (*HVF*) using a plastic matrix. (a) hybrid AS4-Eglass, (b) hybrid M50S-AS4, and (c) hybrid AS4-T800G. The non-hybrid composites are also shown.

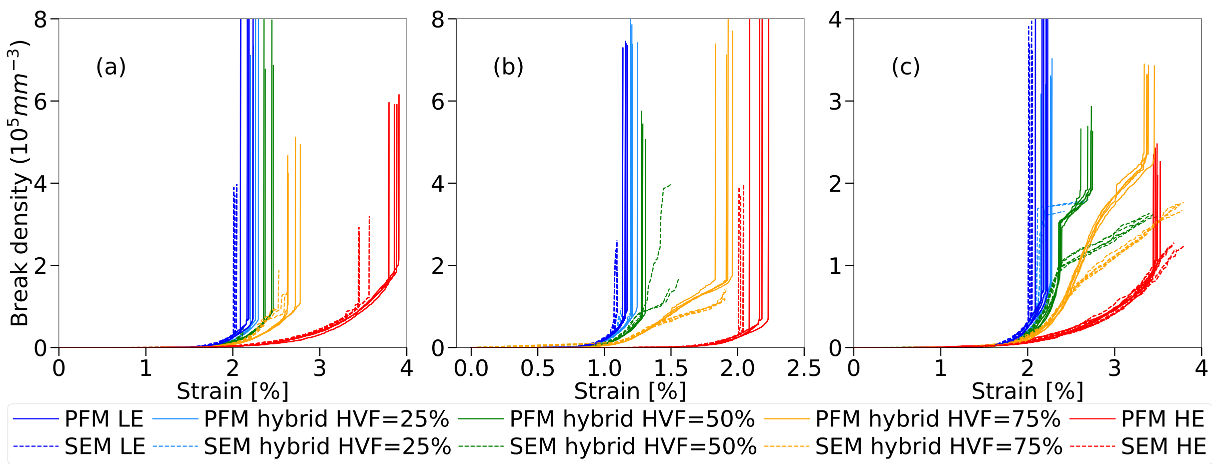

Figure 8: Simulated break-density curves for different hybrid materials at different hybrid volume fractions (*HVF*) using a plastic matrix. (a) hybrid AS4-Eglass, (b) hybrid M50S-AS4, and (c) hybrid AS4-T800G. The non-hybrid composites are also shown.

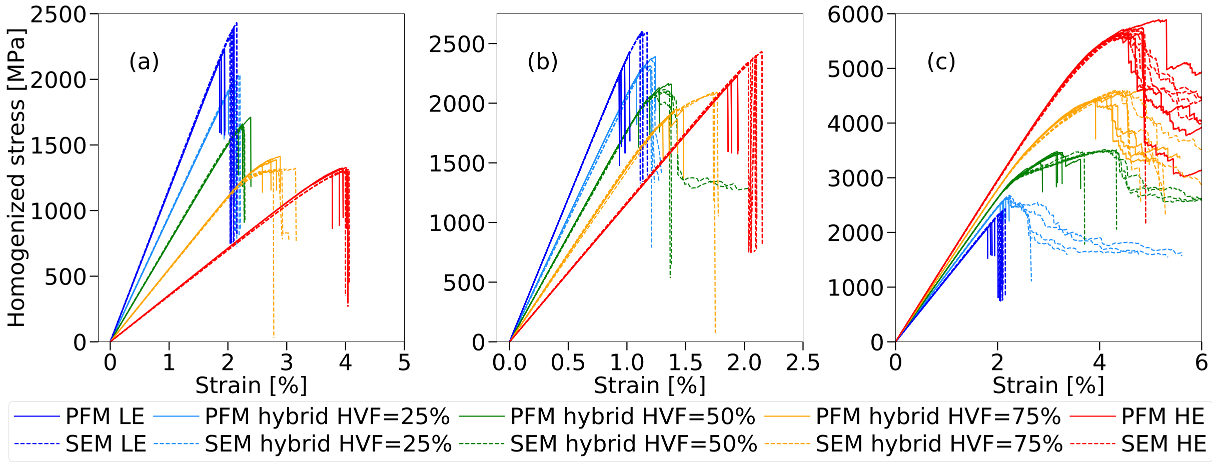

Figure 9: Simulated stress-strain curves for different hybrid materials at different hybrid volume fractions (*HVF*) using an elastic matrix. (a) hybrid AS4-Eglass, (b) hybrid M50S-AS4, and (c) hybrid AS4-T800G. The non-hybrid composites are also shown.

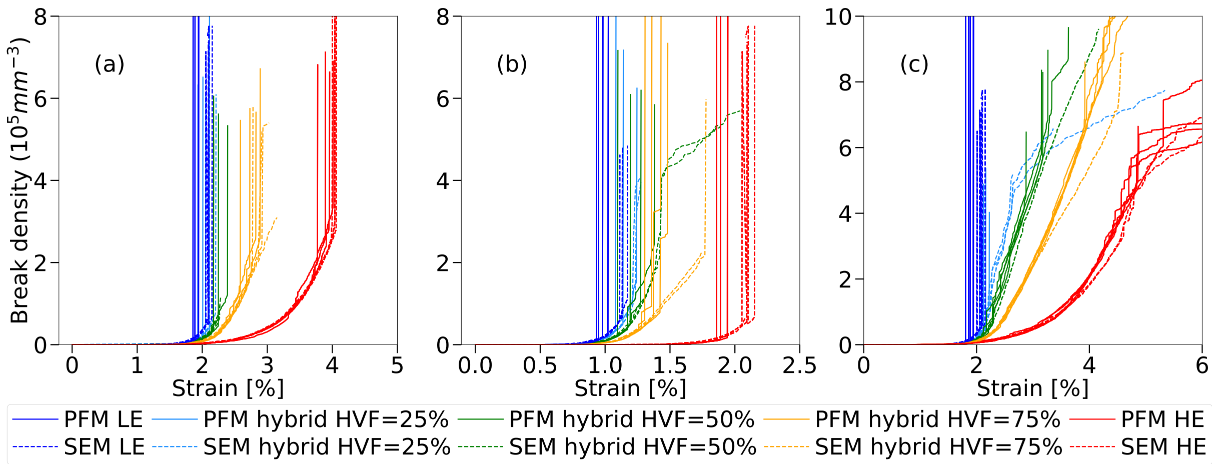

Figure 10: Simulated break-density curves for different hybrid materials at different hybrid volume fractions (*HVF*) using an elastic matrix. (a) hybrid AS4-Eglass, (b) hybrid M50S-AS4, and (c) hybrid AS4-T800G. The non-hybrid composites are also shown.

Table 1: Fibre properties.

Fibre type	Fibre properties		Weibull properties		
	E_f [GPa]	R_f [mm]	m [-]	σ_0 [MPa]	L_0 [mm]
AS4	230	$3.5 \cdot 10^{-3}$	10.7	4275	12.7
M50S	480		9	4600	10
T800G	295		4.8	6800	10
E-glass	70		6.34	1550	24

Table 2: Obtained results for all hybrid materials with plastic matrix.

Material	*HVF*	SEM						PFM					
		σ^y	σ^{ult}	ε^d	ε^{ult}	N^c	δ_f^{ult}	σ^y	σ^{ult}	ε^d	ε^{ult}	N^c	δ_f^{ult}
	[%]	[MPa]	[MPa]	[%]	[%]	[-]	$[1/mm^3]$	[MPa]	[MPa]	[%]	[%]	[-]	$[1/mm^3]$
Hybrid AS4-Eglass	25	1844	1858	0.101	2.026	5.2	2880	2009	2025	0.134	2.251	10.4	6195
	50	1481	1494	0.101	2.067	4.4	2380	1624	1660	0.192	2.388	9.4	6712
	75	1144	1153	0.124	2.201	4.0	2480	1239	1299	0.316	2.653	14.2	8141
Hybrid M50S-AS4	25	2163	2163	0.065	1.098	10.6	4235	2310	2321	0.091	1.199	8.6	7063
	50	1955	1966	0.109	1.210	14.8	6435	2052	2060	0.119	1.275	7.0	6922
	75	1680	1897	0.525	1.808	14.4	9692	1817	2020	0.517	1.893	60.2	16229
Hybrid AS4-T800G	25	2432	2444	0.115	2.076	7.2	3831	2604	2614	0.112	2.223	33.8	6397
	50	2687	2720	0.157	2.213	7.0	4719	2880	2908	0.141	2.345	11.6	7439
	75	2978	3222	0.646	2.949	8.8	10670	3213	3533	0.760	3.282	31.0	21340

Table 3: Obtained results for all hybrid materials with elastic matrix.

Material	*HVF*	SEM						PFM					
		σ^y	σ^{ult}	ε^d	ε^{ult}	N^c	δ_f^{ult}	σ^y	σ^{ult}	ε^d	ε^{ult}	N^c	δ_f^{ult}
	[%]	[MPa]	[MPa]	[%]	[%]	[-]	$[1/mm^3]$	[MPa]	[MPa]	[%]	[%]	[-]	$[1/mm^3]$
Hybrid AS4-Eglass	25	2001	2002	0.070	2.144	16.2	5661	1927	1927	0.022	2.038	9.4	2471
	50	1627	1635	0.102	2.253	18.6	6585	1648	1652	0.061	2.246	77.2	5739
	75	1247	1315	0.531	2.900	135.2	22360	1290	1349	0.221	2.648	132.6	17150
Hybrid M50S-AS4	25	2278	2313	0.074	1.180	30.8	7958	2237	2237	0.039	1.107	33.2	5979
	50	2069	2090	0.157	1.327	34.8	13141	2060	2075	0.064	1.229	116.0	8625
	75	1923	2078	0.299	1.706	42.8	19782	1876	1893	0.069	1.358	80.0	6977
Hybrid AS4-T800G	25	2602	2656	0.063	2.194	49.3	9242	2583	2585	0.042	2.130	115.2	6073
	50	2969	3495	1.557	4.199	4745.0	92451	3006	3414	0.539	3.127	1136.0	56394
	75	3447	4576	1.054	4.326	159.0	63661	3525	4484	0.991	4.192	3909.8	78179

Table 4: Obtained results for all non-hybrid materials with plastic (τ_q = 50) and elastic matrix ($\tau_q = \infty$).

Material	τ_q	SEM						PFM					
		σ^{y}	σ^{ult}	ε^{d}	$\varepsilon^{\mathrm{ult}}$	N^{c}	$\delta_{\mathrm{f}}^{\mathrm{ult}}$	σ^{y}	σ^{ult}	ε^{d}	$\varepsilon^{\mathrm{ult}}$	N^{c}	$\delta_{\mathrm{f}}^{\mathrm{ult}}$
	[MPa]	[MPa]	[MPa]	[%]	[%]	[-]	[$1/mm^3$]	[MPa]	[MPa]	[%]	[%]	[-]	[$1/mm^3$]
AS4	50	2252	2252	0.094	2.018	4.2	3265	2383	2391	0.105	2.172	14.2	5927
	∞	2397	2397	0.065	2.114	14.0	6482	2173	2173	0.009	1.887	8.2	1413
T800G	50	3605	3950	0.377	3.055	3.4	4940	3873	4388	0.416	3.376	6.0	7864
	∞	4615	5613	0.671	4.476	75.5	31195	4725	5708	0.935	4.785	1035.8	45807
M50S	50	2388	2388	0.059	1.054	5.2	3477	2590	2592	0.074	1.150	8.0	7187
	∞	2599	2599	0.058	1.141	17.4	7900	2385	2385	0.015	1.005	5.2	2604
E-glass	50	1043	1111	0.251	3.426	10.6	9479	1168	1263	0.316	3.859	22.0	18335
	∞	1222	1301	0.246	3.964	47.8	26062	1244	1311	0.217	3.895	177.0	25973